Metal matrix to ceramic matrix transition via feedstock processing of SPS titanium composites alloyed with high silicone content

Serhii Tkachenko[1*], Jan Cizek[2], Radek Mušálek[2], Karel Dvořák[3], Zdenek Spotz[1], Edgar B. Montufar[1], Tomáš Chráska[2], Ivan Křupka[1], Ladislav Čelko[1]

[1]Central European Institute of Technology, Brno University of Technology, Purkynova 123, 612 00 Brno, Czech Republic

[2] Institute of Plasma Physics, Academy of Sciences of the Czech Republic, Za Slovankou 1782/3, 182 00 Prague, Czech Republic

[3]AdMaS Center, Faculty of Civil Engineering, Brno University of Technology, Purkynova 139, 612 00 Brno, Czech Republic

*Corresponding author:

Address: CEITEC – BUT, Purkynova 656/123, Brno 612 00, Czech Republic

E-mail: Serhii Tkachenko, Serhii.Tkachenko@ceitec.vutbr.cz

Tel: (+420) 605574708

Abstract

Owing to their excellent mechanical properties and oxidation resistance at high temperatures, sufficient wear resistance, and high chemical stability in various corrosion environments, titanium silicides represent a promising candidate as reinforcement for the development of light-weight composites. In the present paper, titanium-silicone feedstocks were

prepared via three different powder metallurgy routes (milling, blending). As opposed to previous silicide-reinforced Ti studies, high silicone content (20 wt%) was used and the powders were compacted using spark plasma sintering (SPS) technology. In-situ formation of four distinct silicide phases ($TiSi_2$, TiSi, Ti_5Si_4 and Ti_5Si_3) was observed. Interestingly, the microstructure and phase content of the SPS compacts varied significantly with the powder processing route, despite the powders' initial identical composition. Taking advantage of this, composites ranging from relatively soft metal-matrix (52vol.% metallic Ti; using non-milled Ti and coarse or fine-milled Si) to hard ceramic-matrix (11vol.% metallic Ti, using fine-dispersed joint-milled mixture of Ti and Si) were prepared. All the sintered composites showed superior hardness and wear resistance in comparison to pure Ti, though dissimilar wear mechanisms were observed depending on the microstructure of the compacts. Importantly, hardness and elastic modulus of intermediate compounds $TiSi_2$, TiSi, Ti_5Si_4 and Ti_5Si_3 were measured using instrumented indentation technique for the first time and are presented in the paper.

Keywords: intermetallic-strengthened composites; titanium silicides; rapid sintering; nanoindentation; wear

1. Background

Over the last decades, titanium silicides have attracted great attention as structural materials because of superior combination of low density, high temperature strength and excellent oxidation resistance. Among them, Ti_5Si_3 is considered the most perspective owing to its low density of 4.23 g/cm^3, the highest melting temperature (2130 ºC) among the other titanium silicides, high mechanical properties (hardness of 11-12 GPa and elastic modulus of 225 GPa)

(Yeh et al. 2007; Tang et al. 2008). Its excellent oxidation resistance comparable to that of $MoSi_2$ and adequate strength and creep resistance at elevated temperatures further make it attractive for high-temperature structural applications (Frommeyer & Rosenkranz 2004; Vojtěch et al. 2008; Vojtěch et al. 2005). The Ti_5Si_3 compound was also suggested for possible application in the tissue replacements, since the Ti_5Si_3 layer deposited on the surface of Ti-6Al-4V alloy was shown to promote early bonding of Ti implant to bone by inducing a surface apatite layer (Kitsugi et al. 1996). Another important silicide is $TiSi_2$ because it combines high-temperature properties with relatively high thermal and electrical conductivities that make it suitable candidate for diffusion barriers and electronic interconnection applications. However, titanium silicides have limited ductility and low fracture toughness of 2-3 $MPa \cdot m^{1/2}$ (Mitra 1998; Frommeyer & Rosenkranz 2004) at low temperatures due to complex low-symmetry crystal lattices and/or strong covalent bonding between titanium (Ti) and silicon (Si) atoms. This has limited their usage in structural application in bulk condition. Such disadvantage can be minimized by using composite approach, when this intermetallic compound acts as a reinforcement phase, improving the overall hardness, strength, or wear resistance of the entire composite structure, while the ductile Ti phase provides appropriate ductility, fracture toughness and machinability. Ti/Ti_5Si_3 composites have been produced through a variety of methods, including arc melting, vacuum sintering, laser assisted deposition, tungsten inert gas (TIG) surface alloying, reactive sintering or self-propagating high-temperature synthesis (SHS). (Alman & Hawk 1999; Hajbagheri et al. 2008; Alhammad et al. 2008; Tkachenko et al. 2014; Tkachenko et al. 2015; Novák et al. 2010; Novák et al. 2013; Alman 2005). However, manufacturing of these composites using conventional technologies is often accompanied with issues such as excessive grain growth, development of porosity or microstructural

heterogeneities. In this connection, novel sintering methods of composites manufacturing such as spark plasma sintering (SPS) attract great attention due to a number of significant advantages over the conventional powder metallurgy methods and other metallurgical approaches. SPS demonstrates better sintering due to rapid heating rates, short sintering times (thereby limiting the risk of grain growth), and applied external pressure (which improves the densification) (Jia et al. 2014). Previous works on SPS of Ti-Si high-energy ball milled powder mixtures with total Si content in the range of 0-10 wt.% showed high compactness and good mechanical properties of the manufactured Ti/Ti_5Si_3 composite materials (Handtrack et al. 2006; Park et al. 2016). Nonetheless, the effect of the initial powder feedstock parameters on sintering behavior, the features of microstructure formation, and the mechanical properties of the sintered products have not been studied in detail. The aim of this work was to study the mechanism of microstructure formation of the Ti-Si composites during *in situ* SPS synthesis from Ti and Si powders with different particle sizes and morphologies. As opposed to previous papers, the increased amount of Si triggered intensive formation of the Ti-silicide reinforcing phases for the composite mechanical performance and wear resistance improvement.

2. Experimental

2.1. Preparation of powder mixtures

Commercially pure Ti (Sulzer Metco, 11-45 μm) and Si (HC Starck, 20-75 μm) powders (particle size distribution D10-D90 was always reported) were used as initial materials to prepare three series of powder blends with the same Ti/Si powder ratio (Ti-20wt.%Si), but of different

powder particle sizes and preparation process conditions. The designations of the powder blends and their preparation conditions are presented in Table 1. The TS-1 powder blend was prepared through dry mechanical mixing of as-received Ti and Si powders using a jar rolling mixer at 50 rpm for 2.5 h. To obtain the TS-2 powder mixture with finer Si particles, the as-received Si feedstock was milled in a horizontal high energy ball-mill Simoloyer CM01 (Zoz, Germany) at 250 rpm for 10 minutes. Hardened steel balls of 6 mm in diameter were used as the grinding media with the ball-to-powder ratio of 20:1 by weight. The obtained milled Si powder had the particle size 0.5-10 μm and was used to produce the TS-2 powder mixture by mixing it with initial (non-milled) Ti powder. The third powder mixture (TS-3) was produced by joint milling of the initial Ti and Si powders using a planetary ball mill Pulverisette 5 (Fritch, Germany) at the revolutions speed of 220 rpm for a total time of 10 h. Hardened steel balls of 10 mm in diameter were used as grinding media, added with the ball to powder ratio of 10:1 by weight. The milling scheme included 0.5 h of milling followed by 1 h of stoppage for powder cooling. To ensure homogeneous milling and to prevent excessive aggregation of the powders in the stainless-steel jar, 1 wt.% of hexane was added to the system prior to milling. Initial Ti powder was used as a fourth, reference material (denoted as TP).

Table 1. Compositions and processing conditions of powders designated for subsequent SPS sintering.

Material designation	Powder mixture composition	Powder preparation conditions
TP	100wt.% Ti	As-received Ti powder
TS-1	Ti-20wt.%Si	Mixing of initial Ti and Si powder
TS-2	Ti-20wt.%Si	Ball milling of initial Si powder followed by mixing it with initial Ti powder
TS-3	Ti-20wt.%Si	Joint ball milling of initial Ti and Si powders

2.2. In situ synthesis of composites by spark plasma sintering

Ti-Si composites were manufactured by means of SPS technology using SPS 10-4 system (Thermal Technology LLC, USA) equipped with 4000 A DC power supply. Doses of prepared powder mixtures of 7 g were placed into a graphite die of 25 mm inner diameter lined with a carbon foil to prevent adhesion of the samples with the die walls. Using pulses of direct electric current in on/off cycles of 120 ms and 30 ms, respectively, the SPS was carried out in three main stages (Fig. 1):

(I) Degasification of the system at room temperature till a vacuum of 4.5 Pa, heating to 500 °C at a heating rate of 100 ºC/min with 10 minutes dwell time to remove moisture and organic impurities in the powder. Jointly with the heating, a mechanical load was progressively applied up to 60 MPa;

(II) Heating up to the sintering temperature of 1200 °C at a heating rate of 100 ºC/min with a subsequent dwell time of 5 minutes and applied constant load of 60 MPa;

(III) Controlled cooling of 100 ºC/min of the chamber to ambient temperature and progressive relieving of the load.

The temperature of the process was controlled using a K-type thermocouple placed in the die close to the compact surface. Three samples of approximate dimensions 25 x 5 mm were fabricated for each powder mixture for better statistics.

2.3. Microstructural and chemical characterization

The microstructure of the powders and the sintered samples was studied using scanning electron microscope (SEM) Lyra3 (Tescan, Czech Republic) equipped with EDX detector. To reveal the microstructure, the samples were etched with Kroll's reagent composed of 2 vol.% of 40% hydrofluoric acid (HF), 6 vol.% of nitric acid (HNO_3), and 92 vol.% of deionized water (Vander Voort 1984).

Chemical analysis of the samples was done using X-ray Smartlab diffractometer (Rigaku, Japan) set up in the Bragg-Brentano geometry with Cu K_α radiation ($\lambda = 0.154$ nm) operated at the current of 30 mA and voltage of 40 kV. The diffraction pattern was collected from 30° to 90° with the step size of 0.02° and the scanning speed of 4°/min. The Rietveld refinement of the obtained X-ray diffraction (XRD) patterns was performed using X'Pert Highscore v.2a software and the crystallographic models belonging to the detected phases.

2.4. Mechanical characterization

The average hardness of the sintered samples was measured by Vickers indentation method applying the load of 49.03 N (5 kgf) with the dwell time of 15 s using Durascan (Struers, Denmark) microhardness testing machine. The individual results represent the mean of at least 15 measurements. Furthermore, an additional information about the micro-mechanical properties of the composite constituent phases was provided by the instrumented indentation technique. The indentation measurements were performed using the NHT^2 tester (Anton Paar, Austria) equipped with Berkovich indenter. The indentations were done at a maximum load of 50 mN, with loading and unloading rates of 100 mN/s and a dwell time of 15 s. The testing conditions were chosen in order to receive a mechanical response from the site of interest only, effectively limiting the contribution and influence of the adjacent phases. The values of instrumented hardness H_{it} and elastic modulus E_{it} were calculated using proprietary software Indentation v.5.18 (CSM instruments, Switzerland) based on the Oliver-Pharr model (Oliver & Pharr 1992).

The wear testing was done using a commercial UMT TriboLab tribometer (Bruker, USA), using a reciprocal ball-on-plate scheme. Prior to the testing, the disc samples from investigated materials were successively ground with #250-2000 grit SiC papers and finally polished with 1 μm diamond suspension using a linen disc. During the testing, the sample performed reciprocating movement, while a 9.51 mm-diameter alumina (Al_2O_3) counterpart ball was fixed stationary on top of the plate under an applied normal load. Alumina was chosen due to its high hardness and low reactivity. The used parameters of the testing were a normal load of 10 N, stroke length of 10 mm, stroke frequency of 2 Hz and test duration of 20 min (corresponding to a total sliding distance of 24 m). The friction force and sample displacement

were monitored and recorded in-situ. The specific wear rates of the studied materials were quantified according to the Archard's model equation (Archard 1953):

$$(Specific\ wear\ rate = (Wear\ volume)/(Load \cdot Distance)) \quad (1)$$

where the wear volume was calculated as the product of the worn cross-sectional area measured with the optical profilometer ContourGT (Bruker, USA) and the total sliding distance. The coefficients of friction (COF) were calculated as a ratio between the applied normal and friction forces.

3. Results

3.1. Phase composition and morphology of feedstock powders

XRD patterns of the initial powder mixtures designated for the following in situ synthesis of Ti-Si composites are shown in Fig. 2. In general, the detected phases were α-Ti with the hexagonal close packed (HCP) crystal lattice and Si with the face centered diamond cubic lattice. In contrast to TS-1 and TS-2 mixtures, the XRD pattern of the TS-3 powder sample after ball milling showed significant broadening of diffraction peaks for both Ti and Si components, as well as a reduced amount of Si detected (cf. 15.3 wt.% and 19.3 wt.%, 18.4 wt.% in TS-1 and TS-2 mixtures, respectively). Interestingly, the position of the diffraction peaks for both Ti and Si components in all Ti-Si mixtures did not differ in all samples, indicating similarity of their respective lattice parameters.

The morphologies of the powder mixtures obtained through blending and ball milling are presented in Fig. 3. Fig. 3a-c shows the morphology of as-purchased Ti and Si powders in the mixture TS-1. The application of the ball milling to the Si powder has resulted in the reduction of its particle size from 20-75 μm in the TS-1 mixture to 1-20 μm in the TS-2 mixture (cf. Fig. 3 d-f). In contrast, concurrent milling of Ti and Si powders (TS-3) resulted in formation of agglomerates of 2-20 μm in size (Fig. 3g), comprising of fine dispersion of submicron Ti and Si particles. In the agglomerates, both elements were distributed evenly (as could be seen from EDX mapping in Fig. 3h-i), thereby presenting a suitable material for the subsequent process of SPS synthesis.

3.2. Phase composition and microstructure of spark plasma sintered composites

The XRD analysis showed that after SPS, all the samples contained α-Ti with hexagonal close packed (HCP) crystal lattice. In addition, Ti-Si composites (samples TS-1, TS-2 and TS-3) contained various types of Ti-silicides (Fig. 4). The main phases in the sintered TS-1 sample were α-Ti, pure Si with face centered diamond-cubic lattice and Ti-silicide phases identified as Ti_5Si_3, Ti_5Si_4, TiSi, and $TiSi_2$. The composite sample TS-2 contained α-Ti and a smaller variety of silicide phases (Ti_5Si_3, Ti_5Si_4, and TiSi), while TS-3 composite was composed of α-Ti and Ti_5Si_3 phases only, i.e., for both composites sintered from milled powders (TS-2, TS-3) no initial Si or $TiSi_2$ silicides were identified. Furthermore, a characteristic feature of the α-Ti phase in the TS-3 sample was a significant difference in the parameters of the crystal lattice as compared to the same phase in the other two composites ($a = 0.2978$ nm, $c = 0.4862$ nm in TS-3 as vs. $a = 0.2945$ nm, $c = 0.4679$ nm and $a = 0.2946$ nm, $c = 0.4689$ nm in TS-1 and TS-2 samples, respectively). As found out by the Rietveld quantification of the phases (Fig. 5), the amount of α-

Ti was the highest (32.4 wt.%) for the sample TS-1 produced from the mixture of the as-received powders. In contrast, the TS-2 and TS-3 composites obtained from the milled powders showed a reduced percentage of the α-Ti phase (18.3 wt.% and 10.2 wt.%, respectively) and increased amount of silicide compounds.

The typical microstructure of TS-1 composite consisted of silicide reinforcements (with the volume fraction of 48%) embedded in the α-Ti matrix (Fig. 6a-b). The microstructure of the reinforcements exhibited four layers of various intermetallic phases of different thicknesses surrounding non-reacted Si cores. These intermetallic layers exhibited a fine-grain substructure of equiaxed and columnar morphology in inner and outer silicide layers around the Si core, respectively (Fig. 6b). Some pores were observed inside the reinforcements along with frequently observed cracks oriented perpendicularly to the silicide layers' boundaries (Fig. 6c). EDX chemical microanalysis of these reinforcements from the sites (indicated in Fig. 6d) corresponds to the stoichiometry of $TiSi_2$, TiSi, Ti_5Si_4 and Ti_5Si_3 silicides (Table 2). While the $TiSi_2$ and TiSi phases were clearly distinguishable due to their sharp interphase boundaries, the contrast between the Ti_5Si_4 and Ti_5Si_3 phases was relatively poor.

In comparison to TS-1, the microstructure of the TS-2 sample showed a lower amount of the α-Ti phase (with the volume fraction of 23%), while the silicide phases become predominant phase, occupying much larger area (Figs. 5, 7a-b). The silicides retained the multilayered structure and grain substructure as in the case of the sample TS-1, although the number of distinguished layers was reduced to three. The silicide layers analyzed by EDX chemical microanalysis corresponded to the stoichiometry of TiSi, Ti_5Si_4 and Ti_5Si_3 compounds (Table 2). The cracking in silicides in the composite TS-2 was less pronounced than in TS-1 (Fig. 7c), although many micropores could be observed within the silicide phases.

In contrast to TS-1 and TS-2 composites, the microstructure of composite TS-3 almost entirely comprised of the intermetallic Ti_5Si_3 phase (with the total volume fraction of 89%) with no cracks and very low porosity, while the presence of α-Ti in the microstructure was reduced to isolated particles (Figs. 5, 8). It should be noted that, unlike the α-Ti phase in the TS-1, TS-2 composites, these α-Ti particles showed a very fine lath substructure (Fig. 8b).

Table 2. Summary of EDX point chemical microanalysis of SPS sintered Ti-Si composites. The places selected for chemical analysis are indicated in Figs. 6d, 7d, and Fig. 8b for the samples TS-1, TS-2 and TS-3, respectively.

Composite	Element	Chemical composition (wt.%) in the measured site of corresponding phase					
		1 - α-Ti	2 - Ti_5Si_3	3 - Ti_5Si_4	4 - TiSi	5 - $TiSi_2$	6 - Si
TS-1	Ti	93.3	72.3	68.3	54.8	43.6	0.5
	Si	6.7	27.7	31.7	45.2	56.4	99.5
TS-2	Ti	93.2	72.8	64.7	51.9	-	-
	Si	6.8	27.3	35.3	48.1	-	-
TS-3	Ti	91.1	71.9	-	-	-	-
	Si	8.9	28.1	-	-	-	-

3.3. Mechanical properties

The hardness values and the total silicide volume fraction for the SPS sintered Ti-Si composites and the reference Ti sample are shown in Fig. 9. The hardness of TS-1, TS-2 and TS-3

composites increased gradually with higher total content of silicide phases, and was 2.5, 3.6 and 5.6 times higher than that of the pure Ti sample, respectively.

In Table 3, the values of hardness and elastic modulus of the individual phases observed in Figs. 6d, 7d and 8b are summarized. The elemental chemical composition of these phases is shown above in Table 2. For TS-1 composite, the hardness and elastic modulus values of α-Ti matrix were slightly higher as compared to those of pure α-Ti in TP sample. Among the intermetallic phases, TiSi compound showed the highest values of hardness and elastic modulus. Considering the TS-2 composite, the hardness and elastic modulus of α-Ti and detected intermetallic phases Ti_5Si_3, Ti_5Si_4 and TiSi were similar to that in the TS-1 sample. In contrast to the TS-1 and TS-2 samples, α-Ti and Ti_5Si_3 phases in the TS-3 composite showed higher hardness and elastic modulus, showing a clear evidence of the influence of preprocessing of the initial powders by milling on the mechanical properties of SPS sintered composite.

Table 3. Hardness and elastic modulus of individual phases in SPS sintered samples.

Material	H [GPa] and E [GPa] values for the corresponding phases					
	1 - α-Ti (HCP)	2 - Ti_5Si_3 (hexagonal)	3 - Ti_5Si_4 (tetragonal)	4 - TiSi (rhombohedral)	5 - $TiSi_2$ (rhombohedral)	6 - Si (orthorhombic)
TP	H=5.0±0.9; E=133±6	-	-	-	-	-
TS-1	H=5.4±1.0; E=152±14	H=16.4±0.7; E=235±17	H=18.0±0.8; E=241±9	H=17.0±0.7; E=264±5	H=10.7±0.9; E=244±7	H=11.3±1.0; E=159±11
TS-2	H=5.8±0.5; E=151±22	H=16.3±0.7; E=238±14	H=17.4±0.9; E=230±15	H=18.5±0.6; E=255±4	-	-
TS-3	H=14.1±1.2; E=202±15	H=20.5±0.1; E=268±2	-	-	-	-

Fig. 10 shows the wear rates of the reference titanium sample and the SPS sintered Ti-Si composites. While the wear rate of the composite TS-1 was not strongly different as compared to that of pure Ti, the composite TS-2 exhibited slightly higher wear resistance. The composite TS-3 showed an extreme enhancement in the wear resistance, having 44, 42 and 33 times lower wear rate than those of the TP, TS-1 and TS-2 samples, respectively. Figure 11 shows coefficients of fiction (COF) of the studied materials as a function of experiment time. TP, TS-1 and TS-2 samples showed a rapid initial increase and a subsequent slight increment in their COF, along with high variation of COF during the whole experiment. In contrast, the TS-3 composite showed an initial peak in COF, followed by a steady state friction with a much lower scatter in COF as compared to the other studied composite materials. The analysis of the wear tracks after the wear test (Fig. 12a-b) in the TP sample revealed multiple abrasive scratches and delaminated surfaces. In addition, some irregular-shaped debris in the form of particles could also be seen in the wear tracks surface. In the wear tracks of the TS-1 and TS-2 samples, the abrasive scratches were also observed along with severe cracking and chipping of silicide phases (Fig. 12 d, e, g, h). Conversely, the surface of the composite TS-3 showed less scratches, demonstrating much shallower grooves (Fig. 12 j, k), and was also covered with tribolayer. The analysis of the respective alumina counterparts tested in couple with TP, TS-1 and TS-2 samples revealed a great amount of material transfer due to the adhesion (Fig. 12 c, f, i). Unlike the other samples, the wear scar on the alumina counter-part of sample TS-3 contained smooth tribofilms (Fig. 12 l), similar to those observed in the wear track of the sample.

4. Discussion

The present work was focused on revealing the effect of the initial powder components properties (particle size and morphology) on phase/microstructure formation processes and selected mechanical properties of SPS-manufactured Ti-Si composites using microstructural evaluation, Vickers' hardness test, instrumented indentation (for hardness and elastic modulus) and ball-on-disc reciprocal testing (for friction and wear properties).

The preparation of the powder samples suitable for subsequent SPS processing was aimed at obtaining well-mixed blends of Ti and Si components with a variation in the particle size and morphology. As shown by XRD patterns, the formation of titanium silicides (as observed during mechanical alloying of Ti/Si_3N_4 powders (Li et al. 2011)) or other undesirable phases (such as titanium oxides, nitrides or carbides) which can strongly affect the microstructure and the mechanical properties of synthesized composites was avoided during the mixing/milling of the powders. The TS-3 mixture indicated a possible refinement and/or nano-structurization of the Ti and Si powder particles, as evidenced by the strong Ti and Si diffraction peak broadening and the decrease in the peaks intensities. This is congruent with the previous studies (Unifantowicz et al. 2008; Shen et al. 1995) that observed nano-structurization and partial amorphization of the Si powder during ball milling, and could be a reason for the reduction in the amount of detected crystalline Si (from 20 to 15.3 wt.%). For this powder mixture, partial dissolution of Si in α-Ti to form supersaturated solid solution, as in the case of mechanically alloyed Ti-Si powders obtained by Gu et al. (Gu et al. 2004) was not confirmed in our study as the values of the lattice parameters of α-Ti were retained (dissolution of Si into Ti would have caused reduction in the lattice size due to the fact that the atomic radius of Si is smaller than that of Ti). The formation of submicron/nanosized microstructures of TS-2/TS-3 mixtures due to partial/complete milling of

initial Ti and Si components can accelerate diffusion processes during in situ composite synthesis and increase the reaction degree between elemental components, thus affecting the resulting microstructure and the mechanical properties of composites.

As be observed from XRD, SEM and EDX data of the SPS sintered samples, different reaction products can be obtained using Ti and Si initial powders of the same chemistry, but involving various mixing/milling procedures. Given the fact that the melting points of the reactant powders (T_m for Ti and Si are 1670 ºC and 1414 ºC, respectively) and the temperatures of formation of silicides according to the Ti-Si phase diagram (Yang et al. 2007; Massalski et al. 1986) are significantly higher than the used SPS processing temperatures, the synthesis of the silicide phases in these composites should mostly occur in a solid phase. As a result, the type of the forming intermetallic phases, their respective fractions and microstructural distribution are controlled by the mutual solid phase diffusion of the two reactants in the reaction zone within the interparticle space. As confirmed by previous studies on the diffusion kinetics of Ti and Si in silicides (Shimozaki et al. 1997; Chambers et al. 1987), Si diffusion in TiSi and $TiSi_2$ silicides is predominated due to smaller atom size. Thus, the diffusion growth of intermetallic layers in Si powder particles is realized dominantly by the inward diffusion of Si through the silicide compounds.

For the TS-1 composite, the intermetallic phases constituting the multilayered reaction zone between initial Ti and Si powders were produced through a series of intermediate interactions $Ti + Si \rightarrow TiSi_2 \rightarrow TiSi \rightarrow Ti_5Si_4 \rightarrow Ti_5Si_3$, which is similar to those obtained by Trambukis and Munir (Trambukis & Munir 1990) during self-propagating high-temperature synthesis (SHS) of Ti and Si powders. Cockeram and Rapp (Cockeram & Rapp 1995) also reported such formation of a multilayered reaction zone in the Ti–Si diffusion couple maintained at 1423 K for

14 h; however, besides the above-mentioned intermetallic compounds they also detected an interlayer of Ti_3Si phase adjacent to a Ti substrate and a Ti_5Si_3 layer. The absence of Ti_3Si compound in our study could be probably determined by the non-equilibrium conditions of SPS sintering due to the fast heating and short reaction time, in contrast to long exposures for a solid state Ti-Si diffusion couple.

The acceleration of in situ compound synthesis during SPS is achieved for the TS-2 and TS-3 composites due to the reduction of the particles size and the increase in the specific surface area of the powders. This results in a better packing of Ti and Si particles in the mixture and their more extensive contact area, thereby shortening the mean diffusion path and facilitating enhanced diffusion of Si and Ti atoms within the multilayered reaction zone. In the TS-2 composite, this leads to a complete depletion of initial Si phase and the formation of less silicides via the reaction sequence: $TiSi \rightarrow Ti_5Si_4 \rightarrow Ti_5Si_3$. The increased amount of the reacted Si results in the decrease of the fraction of α-Ti phase and the dominance of the silicide phases in the microstructure of this composite as compared to TS-1 that basically means the shift from metallic matric composite to ceramic matrix composite structure. The cracking within some silicide particles in TS-1 and TS-2 composites, as shown in Figs. 5c, 6c, can be attributed to the development of inner stresses occurring due to large difference in the coefficients of thermal expansion (CTE) between the different phases as well as their elastic anisotropy along different crystallographic axes (Samsonov et al. 1979; Frommeyer & Rosenkranz 2004; Schneibel et al. 2004). In this case, the stress relaxation could be accomplished partially via cracking of the brittle silicides and/or via plastic deformation of the ductile α-Ti phase. Obviously, more complex multilayered silicides in TS-1 composite consisting of higher number of silicide phases are more susceptible to cracking than those in TS-2. Also, dominant outward diffusion of Si

atoms from the sites of former Si particles results in the formation of micropores in the silicide phases, so-called Kirkendall type porosity, which was previously reported for in situ synthetized TiAl intermetallics (Jan et al. 2015).

In the TS-3 composite, the use of powder components of sub-micron size and with possible nano/amorphous substructure originated due to the ball milling resulted in the formation of binary mixture of Ti_5Si_3 and α-Ti phases. In contrast to SPSed Ti-16 at.% Si compound which consisted of a mixture of $TiSi_2$, TiSi and Ti_5Si_3 phases (Park et al. 2016), the increased reaction degree between the Ti and the Si powders in our study has prevented synthesis of other intermediate silicides, possibly due to higher sintering temperature, different milling parameters and the resulting difference in size and morphology of Ti/Si powders. According to Ti-Si phase diagram (Yang et al. 2007), the chemical composition of TS-3 composite falls into the hypereutectic composition range, thus it shows respective microstructural features including Ti_5Si_3 matrix and α-Ti+Ti_5Si_3 domains with lath substructure. The formation of such microstructure also indicates a rather intensive diffusion processes of redistribution of components, which were initially homogeneously distributed in the milled Ti/Si powder mixture. The formation of domains of α-Ti phase under such conditions probably leads to the significant increase of its lattice parameters in comparison with α-Ti in the other composites; this interesting fact requires further deeper structural investigation and a separate study will be devoted to its underlying phenomena.

From a viewpoint of potential engineering applications, one of the key mechanical properties of synthesized Ti-Si composites is their high hardness, which characterizes the level of strength and may be correlated with their wear resistance. Hardness of the composites TS-1, TS-2 and TS-3 progressively increased, likely as a result of the increase in the content of hard intermetallic

phases. Such increase in hardness with an increase in the amount of the strengthening phase is generally observed for titanium matrix composites (Xiang et al. 2012; Kim et al. 2013; Choi et al. 2014; Alman & Hawk 1999) and is often connected with an improvement of their abrasive wear resistance. Hardness of the composite TS-3 that consists of ~90% of the intermetallic Ti_5Si_3 phase is virtually approaching the hardness of pure Ti_5Si_3 compound, which reported values range from 9.1 to 12.7 GPa (Mitra 1998; Min et al. 1995; Samsonov et al. 1979; Frommeyer & Rosenkranz 2004) because of the differences in grain size and the presence of processing defects. In our case, the high hardness of TS-3 composite was achieved due to better compactness and the absence of processing microcracks provided by the use of the SPS technology. The obtained results are in good correlation with the previous studies on SPS manufactured composites which showed that an increase in the reaction degree by reduction of the particle size of the reactive powders results in a strength increase in a series of Ti-1.61(wt.%)B_4C composites obtained via SPS process (Jia et al. 2014).

Since the Ti-Si in situ synthesized composites in the present work possessed complex multi-phase microstructure, it is important to know the mechanical properties of the constituent phases in order to predict the bulk mechanical behavior of the composites and purposefully adjust their microstructure and phase composition by changing their manufacturing parameters. Instrumented indentation has been recently applied for the mechanical characterization of the composites across a wide range of the microstructural scales (Yuan et al. 2014; Houdková et al. 2012), providing the possibility to record the basic mechanical properties (hardness, elastic modulus) of the individual composite constituents. To our best knowledge, no instrumented indentation data for Ti_5Si_3, Ti_5Si_4, TiSi and $TiSi_2$ phases can be found in the literature. Among the available data on the mechanical properties of silicides, the data obtained by Frommeyer et al. (Frommeyer &

Rosenkranz 2004) for bulk $TiSi_2$ compound (H = 8.53±0.15 GPa, E = 256±10 GPa) were in agreement with the values of hardness and elastic modulus obtained from the load-displacement curves in this study. Also, the indentation hardness of the Ti_5Si_3 phase was similar to that of fine-grained and microcrack-free Ti_5Si_3 processed by mechanical alloying and hipping (H = 17.1±0.7 GPa) (Thom et al. 1992). The indentation of the reinforcements cores which correspond to non-reacted Si gave the values of hardness and elastic modulus (H = 12.2±1.0 GPa, E = 159±11 GPa) that were close to those obtained earlier by Jang et al. (Jang et al. 2005) (H = 11.5-12.5 GPa, E = 160 GPa). The somewhat surprising high values of hardness and elastic modulus of the α-Ti phase in the composite TS-3 may actually represent the composite properties of α-Ti+Ti_5Si_3 lath structure, whose phase and microstructural features were discussed above. This α-Ti+Ti_5Si_3 lath structure was very fine that even at relatively low indentation force of 50 mN two phases have always been indented, so it was not possible to measure the properties of individual phase constituents.

Because sliding contact occurs in many engineering applications, another focus of the presented study was the evaluation of tribological properties of the in situ synthesized Ti-Si composites. Interestingly, analysis of wear and friction data revealed that the wear resistance of the Ti-Si composites was not directly related to the content of hard phases or composite average hardness. This is specifically demonstrated by the marked difference in the wear resistance of the TS-3 sample and the other produced Ti-Si composites. Such tribological behavior is not consistent with what is typically observed for titanium matrix composites reinforced with hard phases, which show progressive decrease in their wear rates and COF with a gradual increase in the hard phases content and, accordingly, composite average hardness (Kim et al. 2013; Kim et al. 2011). The main reason for this phenomenon lies in the significant difference in the wear mechanisms

of the tested Ti-Si composites. SEM analysis of the worn sample surfaces revealed that the dominant wear mechanism for TS-1 and TS-2 composites was abrasive wear due to the formation of wear debris. The formation of the wear debris occurred mostly through the cracking and spalling of the complex multiphase silicide reinforcements which have low mechanical stability at high contact loads during sliding and further contain a network of inner microcracks. The generated wear debris gets entrapped between the mating surfaces, producing severe third-body abrasive action and preventing the formation of protective oxide tribofilms. Such oxide-rich tribofilms are observed to develop on the friction surfaces of titanium matrix composites during sliding (Sun et al. 2010; Xu et al. 2015) under certain experiment conditions (load and sliding speed). They mainly consist of mechanically mixed and oxidized wear debris from the composite constituents (both matrix and reinforcement phases), forming well-consolidated layers on the mating surfaces. In that way, the direct contact of sample and counter-part friction surfaces is transformed to a contact between tribofilms, which is accomplished through the low-shear-strength junctions at the contact interface that give antifriction property and protection against excessive abrasive wear and delamination. In the case of TS-1 and TS-2 composites, protective tribofilms could not form due to their continual removal with wear debris, though some amount of material transfer due to adhesion of the Ti phase to the counter-part was detected on the counter-part surfaces (Fig. 12g, j). The formation of similar transferred material patches was previously associated with high fluctuations in COF in pure Ti and Ti-Si-Zr alloys (Dong & Bell 2000; Tkachenko et al. 2014). Less susceptibility to cracking of the silicides in the composite TS-2 as compared to TS-1 resulted in a slightly lower wear rate due to less intensive three-body abrasive wear. However, both TS-1 and TS-2 composites in general showed wear

rates similar to that of pure Ti, which revealed a dominant wear mechanism as a well-recorded combination of abrasive and oxidation wear (Anon 2015).

In the case of the TS-3 composite, high mechanical stability and the absence of cracks in the silicide phase enabled the formation of protective tribofilms on both mating surfaces of the sample/counter-part tribocouple (Fig. 12 l, m). The tribofilm formation may probably occur at the onset of the friction process accompanied by the COF increase, when under the applied contact pressure, the Ti_5Si_3 and Ti phases get strained to the contact interface and undergo multiple mechanical mixing and associated oxidation during subsequent friction. As a result, well-consolidated tribofilms with high covering percentage, consisting mainly of the mechanically mixed Ti-Si oxides, are formed on both counter-parts and prevent their direct contact. These oxide-rich tribofilms, consisting of the mixed oxide wear debris and being relatively soft and flowable during sliding friction due to high porosity (Huang et al. 2007), effectively support low and stable friction behavior of the TS-3 composite along with its remarkable wear resistance as compared to the rest of studied materials. In this context, in order to obtain high wear resistance and stable friction behavior, the microstructure of the TS-3 composite with higher mechanical stability and ability to form protective tribofilms is preferred over the complex multiphase microstructures of TS-1 and TS-2 composites, which are susceptible to cracking and formation of highly abrasive wear debris during sliding.

The presented results on the mechanical performance of SPS sintered Ti/Si composites indicate their high versatility depending on the compacts microstructure, which changed from metal matrix type in TS-1 to ceramic matrix type in TS-2 and TS-3 composites. This greatly extends the application potential of these composites, enabling a possible use as load-bearing and wear resistant materials. It should, however, be noted that strengthening by brittle phases generally

introduces a significant reduction in crack resistance, inherent mainly to ceramic matrix composites. A separate, extended study on evaluation of fracture toughness of the fabricated Ti/Si composites is currently in progress.

5. Conclusions

In this work, spark plasma sintering was successfully employed to fabricate a series of titanium-silicide composites from Ti-20wt.%Si powder mixtures with different parameters of powder feedstock in terms of the respective particle sizes and morphology. The composite microstructure development involved *in situ* intermetallic formation due to solid state chemical reactions between the Ti and Si particles and their further densification during SPS. The use of the powder mixture with coarse initial Ti and Si particles has resulted in the formation of Ti matrix composite reinforced with complex multiphase silicides that were composed of successive layers of Ti_5Si_3, Ti_5Si_4, TiSi, $TiSi_2$ and pure Si cores. The shift from metallic matrix to ceramic matrix composite occurs when using a powder blend with finer Si particles (1-10 μm). This results in the development of composite microstructure of ceramic matrix, which comprises the mixture of Ti_5Si_3, Ti_5Si_4, TiSi compounds, and Ti phase reinforcements. The use of jointly milled finer Ti and Si powders (with the size below 1 μm) led to the formation of Ti_5Si_3 compound almost throughout the entire sample volume that resulted in a sharp hardness increase. The sintered composites showed improved hardness and wear resistance in comparison to pure Ti, which is due to high content of intermetallic phases with high hardness and elastic modulus evaluated by means of instrumented indentation. The most interesting material for potential engineering applications is the composite with the microstructure consisting of a mixture of Ti_5Si_3 and α-Ti phases, which possess both high hardness, remarkable wear resistance

and stable friction under dry reciprocating sliding. The formation of multiphase silicides, as observed in other Ti-Si composites, is undesirable due to deterioration of friction and wear characteristics of the composite, since these complex layered phases serve as a source of abrasive particles due to spalling during wear testing.

Acknowledgements

This study was carried out under the project CEITEC 2020 (LQ1601) with the financial support from Ministry of Education, Youth and Sports of Czech Republic under National Sustainability Program II. The authors would also like to acknowledge the founding from the European Union's Horizon 2020 research and innovation programme under the Marie Skłodowska-Curie and, co-financed by the South Moravian Region under grant agreement No. 665860.

References

Alhammad, M., Esmaeili, S. & Toyserkani, E., 2008. Surface modification of Ti–6Al–4V alloy using laser-assisted deposition of a Ti–Si compound. *Surface and Coatings Technology*, 203(1), pp.1–8.

Alman, D. & Hawk, J., 1999. The abrasive wear of sintered titanium matrix–ceramic particle reinforced composites. *Wear*, 225, pp.629–639.

Alman, D.E., 2005. Reactive sintering of TiAl–Ti5Si3 in situ composites. *Intermetallics*, 13(6), pp.572–579. Available at: http://www.sciencedirect.com/science/article/pii/S0966979504003164 [Accessed May 31,

2017].

Anon, 2015. Comparison of wear properties of commercially pure titanium prepared by selective laser melting and casting processes. Materials Letters, 142, pp.38–41. Available at: http://www.sciencedirect.com/science/article/pii/S0167577X14021594 [Accessed October 25, 2017].

Archard, J.F., 1953. Contact and rubbing of flat surfaces. Journal of Applied Physics, 24(8), pp.981–988.

Cockeram, B. V & Rapp, R.A., 1995. The kinetics of multilayered titanium-silicide coatings grown by the pack cementation method. Metallurgical and Materials Transactions A, 26(4), pp.777–791. Available at: http://dx.doi.org/10.1007/BF02649076.

Dong, H. & Bell, T., 2000. Enhanced wear resistance of titanium surfaces by a new thermal oxidation treatment. Wear, 238(2), pp.131–137.

Frommeyer, G. & Rosenkranz, R., 2004. Structures and Properties of the Refractory Silicides Ti5Si3 and TiSi2 and Ti-Si-(Al) Eutectic Alloys. In O. N. Senkov, D. B. Miracle, & S. A. Firstov, eds. Metallic Materials with High Structural Efficiency. Dordrecht: Springer Netherlands, pp. 287–308. Available at: http://dx.doi.org/10.1007/1-4020-2112-7_30.

Gu, Y.W. et al., 2004. Structural evolution in Ti-Si alloy synthesized by mechanical alloying. Physica B: Condensed Matter, 352(1–4), pp.299–304. Available at: http://linkinghub.elsevier.com/retrieve/pii/S092145260400849X [Accessed June 29, 2017].

Hajbagheri, F.A., Kashani Bozorg, S.F. & Amadeh, A.A., 2008. Microstructure and wear assessment of TIG surface alloying of CP-titanium with silicon. Journal of Materials

Science, 43(17), pp.5720–5727. Available at: http://dx.doi.org/10.1007/s10853-008-2890-9.

Handtrack, D. et al., 2006. Fabrication of ultra-fine grained and dispersion-strengthened titanium materials by spark plasma sintering. Materials Science and Engineering: A, 437(2), pp.423–429. Available at: http://www.sciencedirect.com/science/article/pii/S0921509306017254 [Accessed April 3, 2017].

Houdková, Š. et al., 2012. The Instrumented Indentation Study of HVOF-Sprayed Hardmetal Coatings. Journal of Thermal Spray Technology, 21(1), pp.77–85. Available at: http://dx.doi.org/10.1007/s11666-011-9677-2.

Huang, Z. et al., 2007. Oxide-film-dependent tribological behaviors of Ti3SiC2. Wear, 262(9), pp.1079–1085. Available at: http://www.sciencedirect.com/science/article/pii/S0043164806004455.

Chambers, S.A. et al., 1987. Silicide formation at the Ti/Si (111) interface: Diffusion parameters and behavior at elevated temperatures. Phys. Rev. B, 35(2), pp.634–640. Available at: https://link.aps.org/doi/10.1103/PhysRevB.35.634.

Choi, B.-J. et al., 2014. Microstructure and friction/wear behavior of (TiB+TiC) particulate-reinforced titanium matrix composites. Wear, 318(1), pp.68–77.

Jan, V., Čupera, J. & Cizek, J., 2015. On the search for producing intermetallics by diffusion reaction of cold spray bulk deposits. Surface and Coatings Technology, 268, pp.216–223. Available at: http://linkinghub.elsevier.com/retrieve/pii/S0257897214011438 [Accessed August 10, 2017].

Jang, J. et al., 2005. Indentation-induced phase transformations in silicon: influences of load, rate

and indenter angle on the transformation behavior. Acta Materialia, 53(6), pp.1759–1770. Available at: http://www.sciencedirect.com/science/article/pii/S135964540400761X [Accessed May 30, 2017].

Jia, L. et al., 2014. Size effect of B4C powders on metallurgical reaction and resulting tensile properties of Ti matrix composites by in-situ reaction from Ti–B4C system under a relatively low temperature. Materials Science and Engineering: A, 614, pp.129–135.

Kim, I.Y. et al., 2011. Friction and wear behavior of titanium matrix (TiB+TiC) composites. Wear, 271(9), pp.1962–1965.

Kim, J.-S. et al., 2013. Fretting wear characteristics of titanium matrix composites reinforced by titanium boride and titanium carbide particulates. Wear, 301(1), pp.562–568.

Kitsugi, T. et al., 1996. Bone bonding behavior of titanium and its alloys when coated with titanium oxide (TiO2) and titanium silicate (Ti5Si3). Journal of Biomedical Materials Research, 32(2), pp.149–156. Available at: http://doi.wiley.com/10.1002/%28SICI%291097-4636%28199610%2932%3A2%3C149%3A%3AAID-JBM1%3E3.0.CO%3B2-T [Accessed August 15, 2017].

Li, C. et al., 2011. In Situ Synthesis of Ti5Si3 Matrix Nanocomposites Reinforced with Nanoparticles by High-Energy Mechanical Alloying. Advanced Engineering Materials, 13(5), pp.418–425. Available at: http://doi.wiley.com/10.1002/adem.201000377 [Accessed August 15, 2017].

Massalski, T.B. et al., 1986. Binary alloy phase diagrams, American Society for Metals. Available at: https://books.google.cz/books?id=9J4RAQAAMAAJ.

Min, K.S. et al., 1995. A small-specimen investigation of the fracture toughness of Ti5Si3. Journal of Materials Science, 30(21), pp.5479–5483. Available at: http://dx.doi.org/10.1007/BF00351561.

Mitra, R., 1998. Microstructure and mechanical behavior of reaction hot-pressed titanium silicide and titanium silicide-based alloys and composites. Metallurgical and Materials Transactions A, 29(6), pp.1629–1641. Available at: http://dx.doi.org/10.1007/s11661-998-0086-1.

Novák, P. et al., 2010. High-temperature behaviour of Ti–Al–Si alloys produced by reactive sintering. Journal of Alloys and Compounds, 504(2), pp.320–324. Available at: http://www.sciencedirect.com/science/article/pii/S0925838810013228 [Accessed March 10, 2016].

Novák, P. et al., 2013. Structure and properties of Ti–Al–Si-X alloys produced by SHS method. Intermetallics, 39, pp.11–19. Available at: http://linkinghub.elsevier.com/retrieve/pii/S0966979513000812 [Accessed August 15, 2017].

Oliver, W.C. & Pharr, G.M., 1992. An improved technique for determining hardness and elastic modulus using load and displacement sensing indentation experiments. Journal of Materials Research, 7(6), pp.1564–1583. Available at: http://www.journals.cambridge.org/abstract_S0884291400017039 [Accessed May 29, 2017].

Park, H.-K. et al., 2016. One step synthesis and densification of Titanium-silicon compounds by a spark plasma sintering method and their mechanical properties. Journal of Ceramic

Processing Research, 17(3), pp.191–196.

Samsonov, G. V., Dvorina, L.A. & Rud', B. V., 1979. Silicides Metallurgy., Moscow.

Shen, T.D. et al., 1995. The structure and property characteristics of amorphous/nanocrystalline silicon produced by ball milling. Journal of Materials Research, 10(1), pp.139–148. Available at: http://www.journals.cambridge.org/abstract_S0884291400076573 [Accessed October 20, 2017].

Shimozaki, T. et al., 1997. Effect of Impurities on Growth of Ti Silicides in Bulk Ti/Si Diffusion Couple. Materials Transactions, JIM, 38(10), pp.865–870.

Schneibel, J.H. et al., 2004. Controlling the thermal expansion anisotropy of Mo5Si3 and Ti5Si3 silicides. Intermetallics, 12(7), pp.845–850. Available at: http://www.sciencedirect.com/science/article/pii/S0966979504000676.

Sun, T. et al., 2010. Study on dry sliding friction and wear properties of Ti2AlN/TiAl composite. Wear, 268(5), pp.693–699. Available at: http://www.sciencedirect.com/science/article/pii/S004316480900595X.

Tang, Z. et al., 2008. High temperature oxidation behavior of Ti5Si3-based intermetallics. Intermetallics, 16(9), pp.1118–1124. Available at: http://www.sciencedirect.com/science/article/pii/S0966979508001428.

Thom, A.J., Kim, Y. & Akinc, M., 1992. Effect of Processing on Oxidation of Ti5Si3. MRS Proceedings, 288.

Tkachenko, S. et al., 2015. Tribological performance of Ti–Si based in situ composites. Tribology Transactions, pp.1–40. Available at:

http://dx.doi.org/10.1080/10402004.2015.1079347.

Tkachenko, S. et al., 2014. Wear and friction properties of experimental Ti–Si–Zr alloys for biomedical applications. Journal of the Mechanical Behavior of Biomedical Materials, 39, pp.61–72. Available at: http://www.sciencedirect.com/science/article/pii/S1751616114002045 [Accessed October 14, 2015].

Trambukis, J. & Munir, Z.A., 1990. Effect of Particle Dispersion on the Mechanism of Combustion Synthesis of Titanium Silicide. Journal of the American Ceramic Society, 73(5), pp.1240–1245. Available at: http://doi.wiley.com/10.1111/j.1151-2916.1990.tb05186.x [Accessed May 31, 2017].

Unifantowicz, P. et al., 2008. Structural changes of silicon upon high-energy milling investigated by Raman spectroscopy. Journal of Physics: Condensed Matter, 20(2), p.25205. Available at: http://stacks.iop.org/0953-8984/20/i=2/a=025205?key=crossref.dd393d7a36e44dd6bc9051ee3bc04a27.

Vojtěch, D. et al., 2005. Influence of silicon on high-temperature cyclic oxidation behaviour of titanium. Journal of Alloys and Compounds, 394(1–2), pp.240–249. Available at: http://www.sciencedirect.com/science/article/pii/S0925838804014410 [Accessed September 25, 2015].

Vojtěch, D. et al., 2008. Surface protection of titanium by Ti5Si3 silicide layer prepared by combination of vapour phase siliconizing and heat treatment. Journal of Alloys and Compounds, 464(1), pp.179–184.

Vander Voort, G.F., 1984. Metallography, Principles and Practice, ASM International.

Available at: https://books.google.com.ua/books?id=GRQC8zYqtBIC.

Xiang, W. et al., 2012. Effect of boron addition on microstructure and mechanical properties of TiC/Ti6Al4V composites. Materials & Design (1980-2015), 36, pp.41–46. Available at: http://www.sciencedirect.com/science/article/pii/S0261306911007424 [Accessed May 30, 2017].

Xu, Z. et al., 2015. Sliding Speed and Load Dependence of Tribological Properties of Ti3SiC2/TiAl Composite. Tribology Transactions, 58(1), pp.87–96. Available at: http://dx.doi.org/10.1080/10402004.2014.951748.

Yang, Y., Bewlay, B.P. & Chang, Y.A., 2007. Thermodynamic modeling of the Hf–Ti–Si ternary system. Intermetallics, 15(2), pp.168–176. Available at: http://www.sciencedirect.com/science/article/pii/S0966979506001853.

Yeh, C.L., Chen, W.H. & Hsu, C.C., 2007. Formation of titanium silicides Ti5Si3 and TiSi2 by self-propagating combustion synthesis. Journal of Alloys and Compounds, 432(1), pp.90–95. Available at: http://www.sciencedirect.com/science/article/pii/S0925838806006645.

Yuan, Z. et al., 2014. Mechanical properties study of particles reinforced aluminum matrix composites by micro-indentation experiments. Chinese Journal of Aeronautics, 27(2), pp.397–406. Available at: http://www.sciencedirect.com/science/article/pii/S1000936114000193 [Accessed May 29, 2017].

Figure 1. Unified pressure and temperature development used in the SPS compaction process.

Figure 2. XRD patterns of prepared powder mixtures (a) TS-1, (b) TS-2 and (c) TS-3 prior to sintering.

Figure 3. SEM SE micrographs (left) and EDX element mapping of Ti (middle) and Si (right) of (a-c) TS-1 powder mixture, (d-f) TS-2 powder mixture, and (g-i) TS-3 powder mixture.

Figure 4. XRD patterns of SPS sintered Ti-Si samples by SPS (a) TP, (b) TS-1, (c) TS-2, and (d) TS-3.

Figure 5. Phase content of the sintered Ti-Si composites determined by Rietveld analysis of the XRD patterns.

Figure 6. SEM BSE micrographs (a-d) and EDX elemental mapping for Ti (e) and Si (f) in the area observed in (d) of the composite TS-1. Frequently observed cracks in the silicide phases surrounding the Si reinforcement particles are indicated with white arrows in (c).

Figure 7. SEM BSE micrographs (a-d) and EDX elemental mapping for Ti (e) and Si (f) in the area observed in (d) of the composite TS-2. Observed cracks in the silicide phases are marked with white arrows.

Figure 8. SEM BSE micrographs (a-b) and EDX elemental mapping for Ti (c) and Si (d) in the area observed in (b) of the composite TS-3.

Figure 9. Hardness and total silicide content of sintered samples.

Figure 10. Wear rates of SPS sintered samples.

Figure 11. Coefficient of friction as a function of experiment time for (a) TP, (b) TS-1, (c) TS-2 and (d) TS-3 SPS samples.

Figure 12. Micrographs of the wear tracks on (a, b) TP, (d, e) TS-1, (g, h) TS-2 and (j, k) TS-3 sample surface, respectively, with their respective wear scars (c, f, i, l) on the alumina ball counterparts.

Research highlights

1. In-situ synthesis of Ti composites alloyed with high Si content achieved via SPS
2. Feedstock powder blend processed via three PM processing routes
3. SPS compacts phase composition significantly affected by the selected route
4. Superior sliding wear resistance was recorded for the silicide-reinforced matrices
5. Nanoindentation properties of Ti_5Si_3, Ti_5Si_4, TiSi and $TiSi_2$ phases are disclosed

Figure 1
Click here to download high resolution image

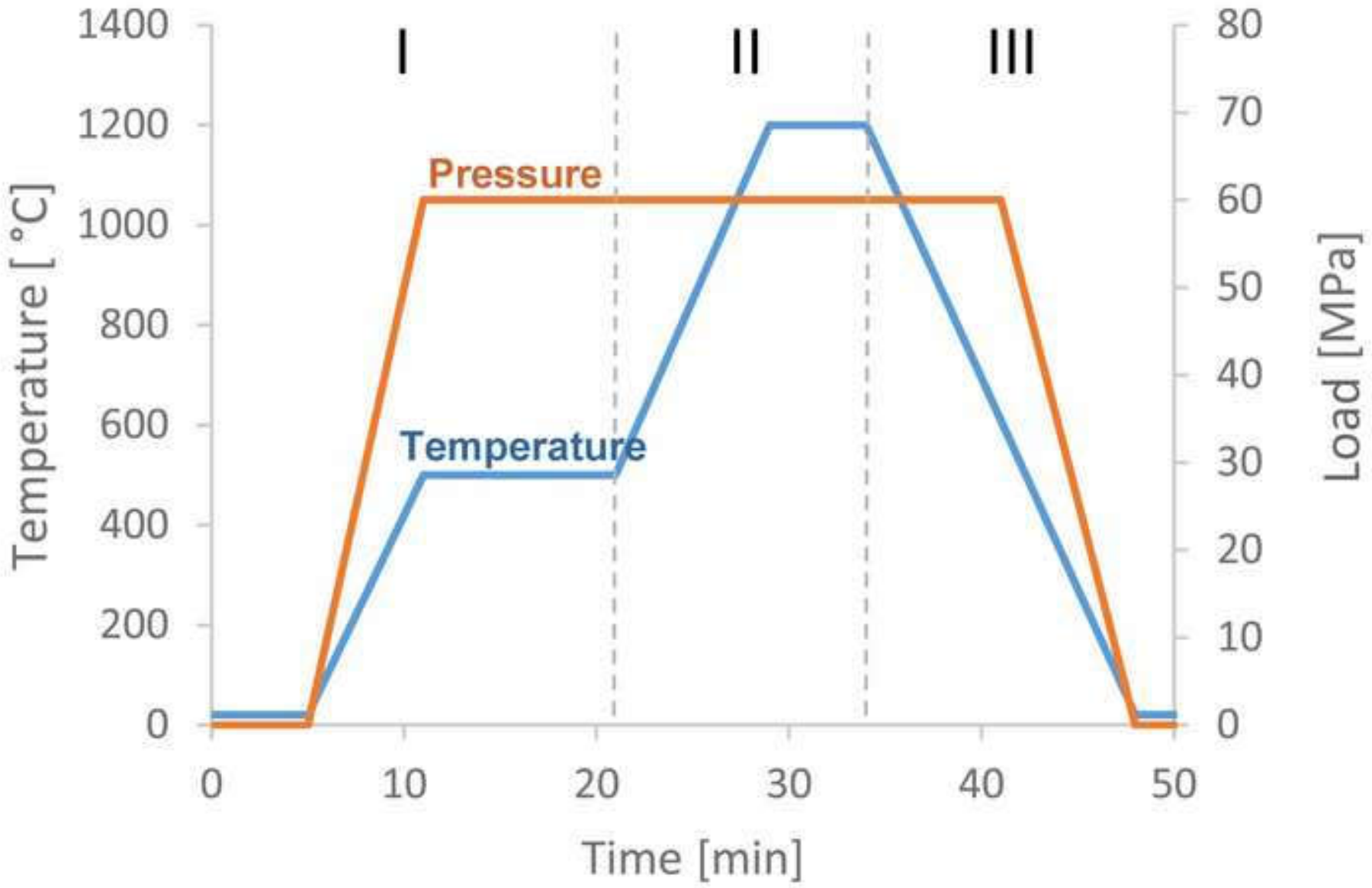

Figure 2

Click here to download high resolution image

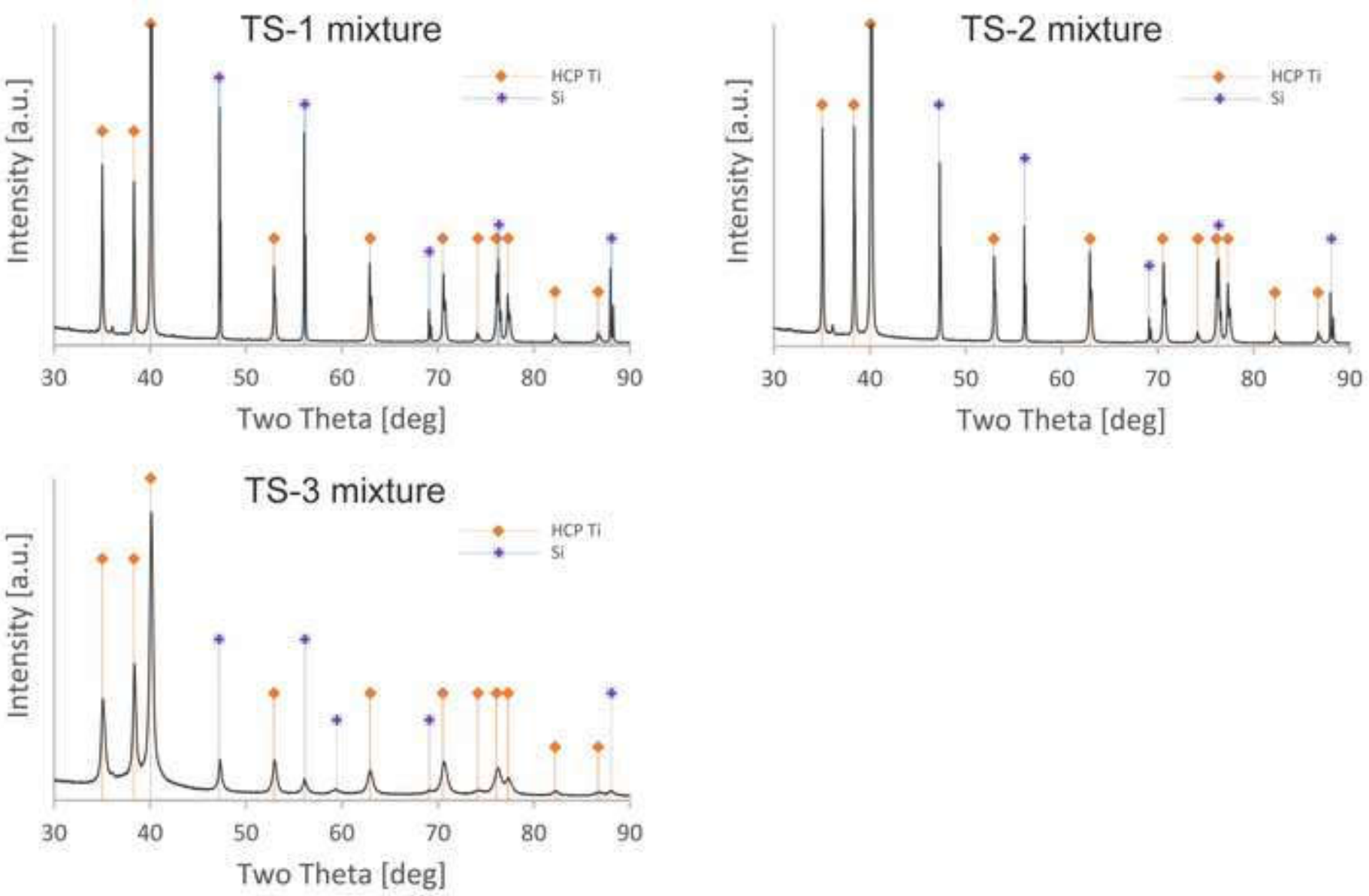

Figure 3
Click here to download high resolution image

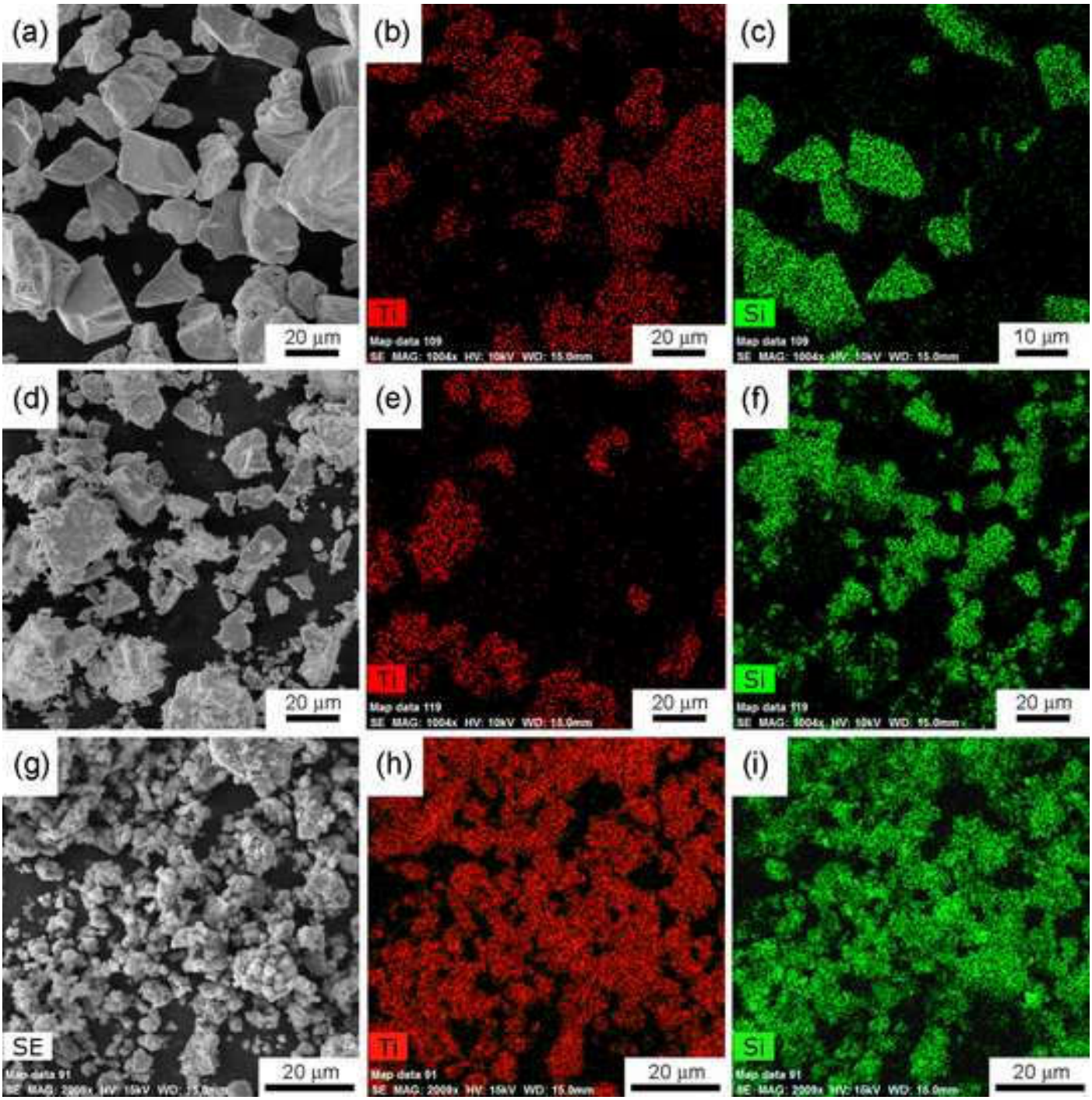

Figure 4

Click here to download high resolution image

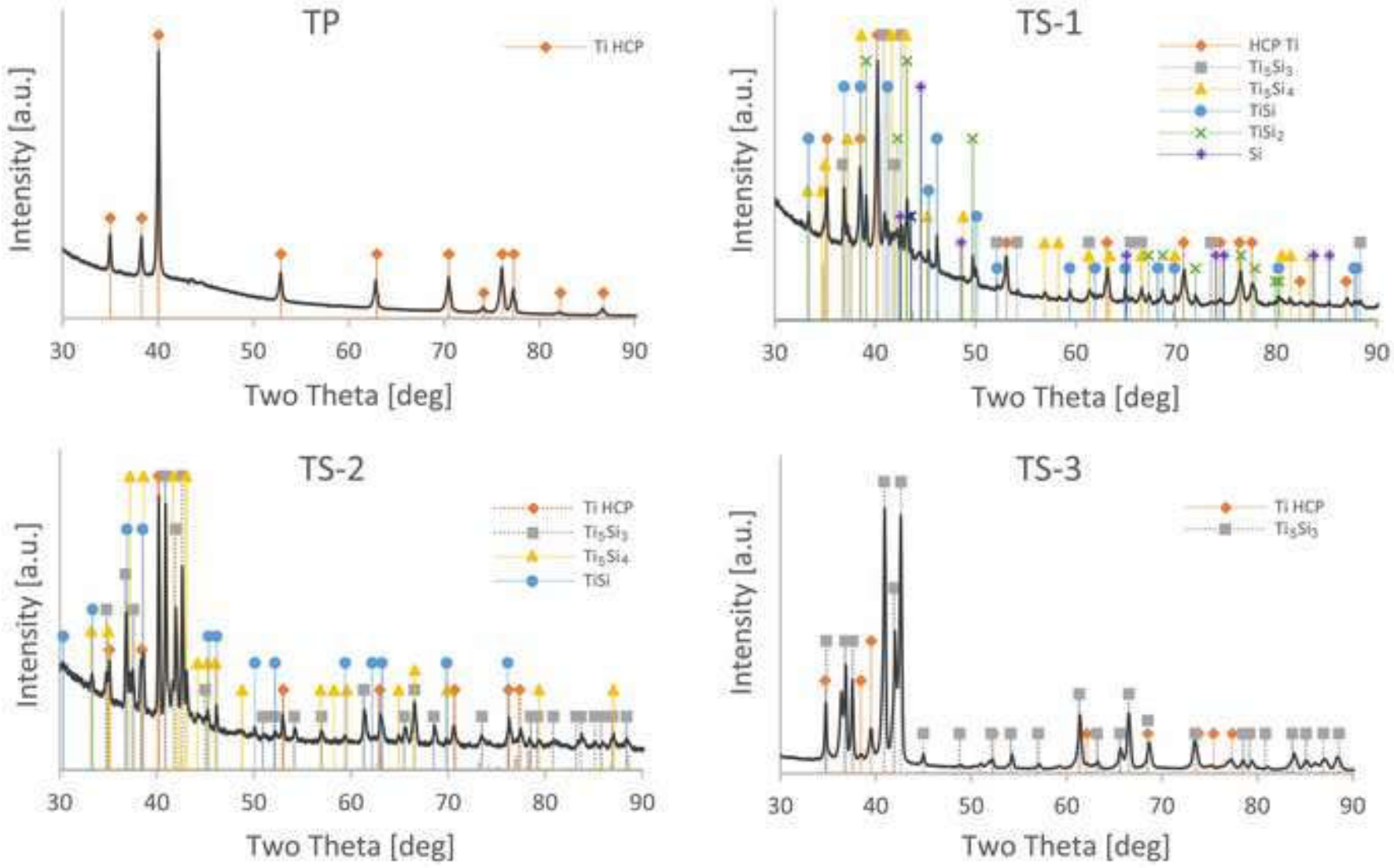

Figure 5
Click here to download high resolution image

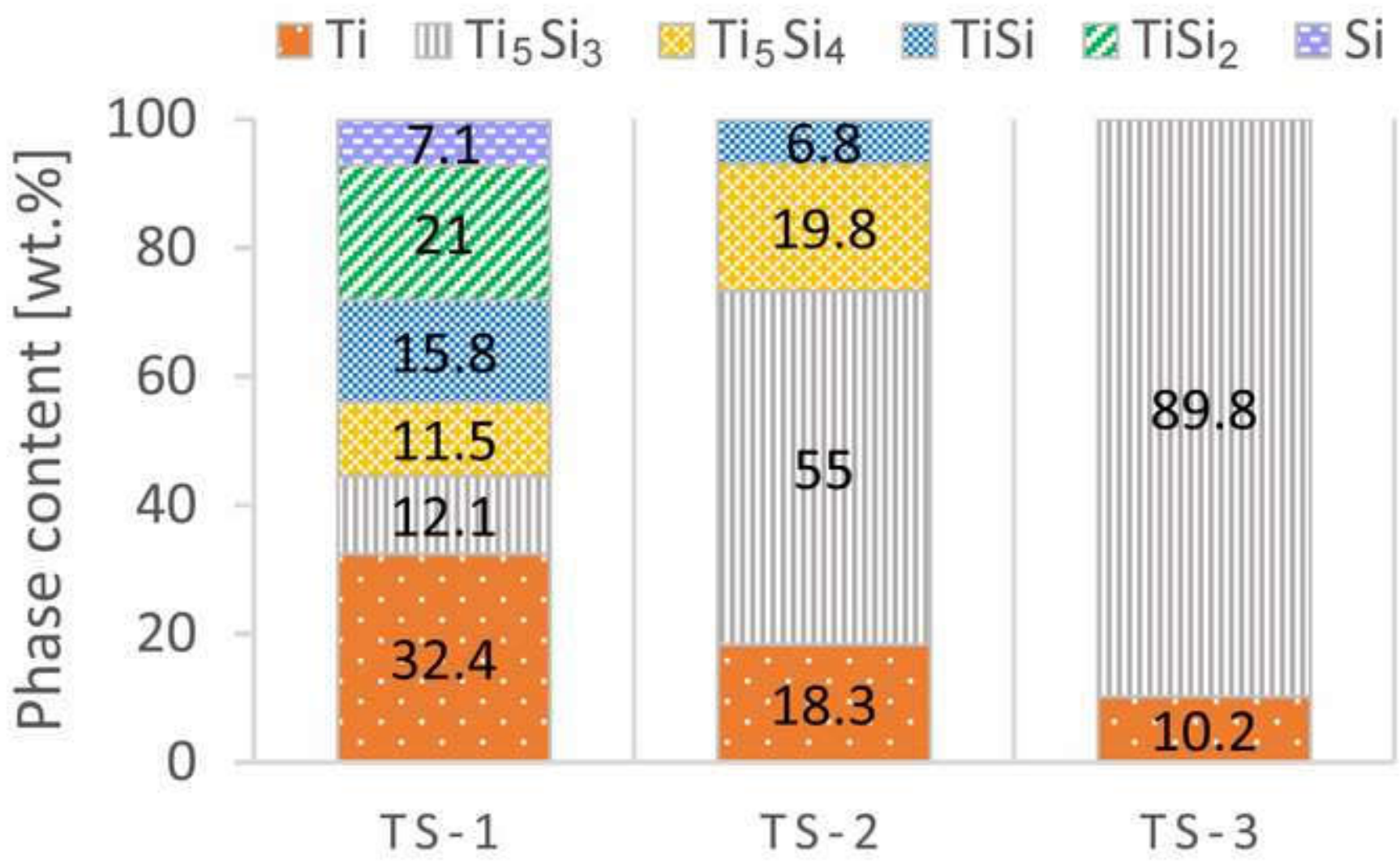

Figure 6
Click here to download high resolution image

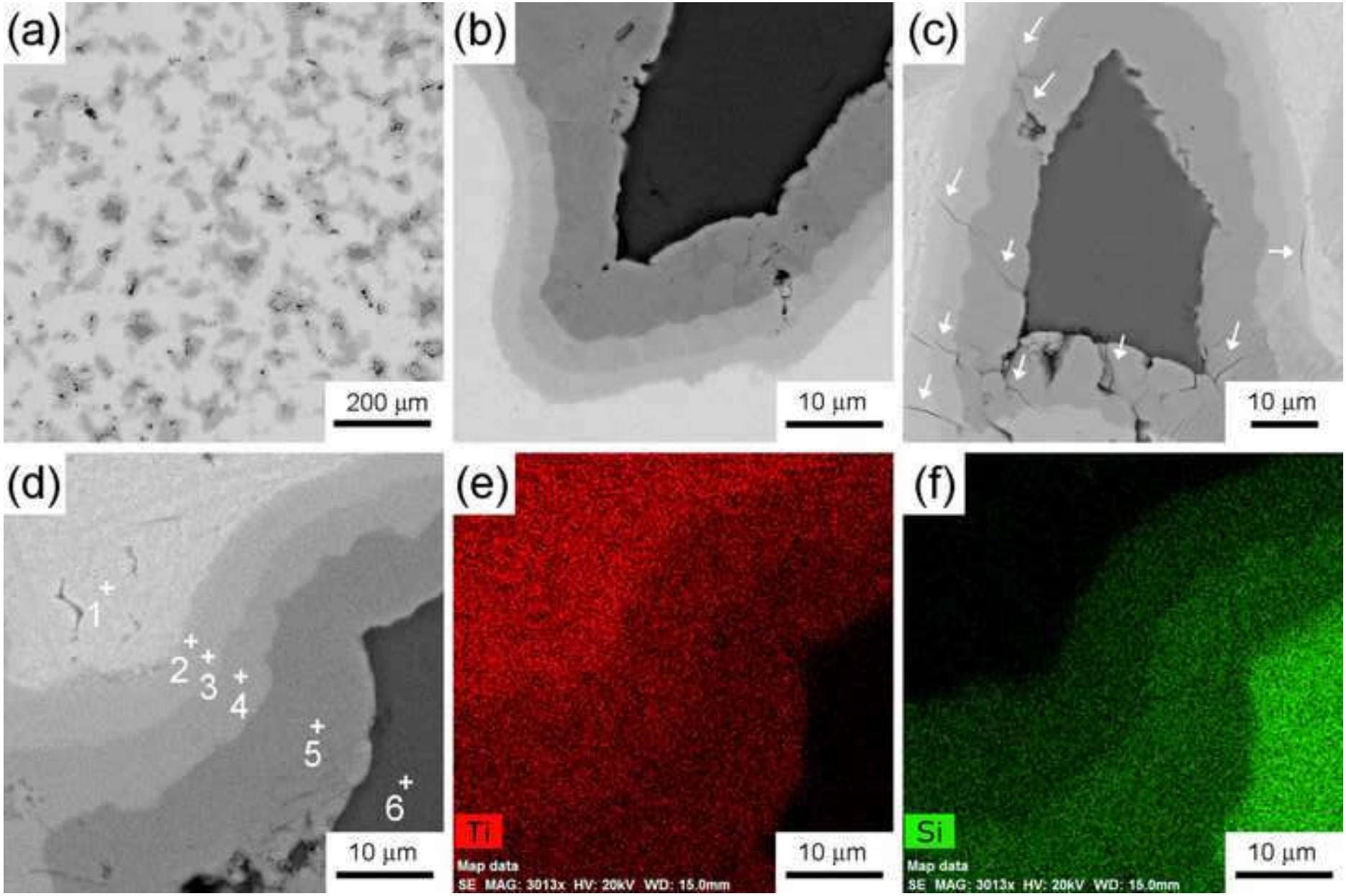

Figure 7
Click here to download high resolution image

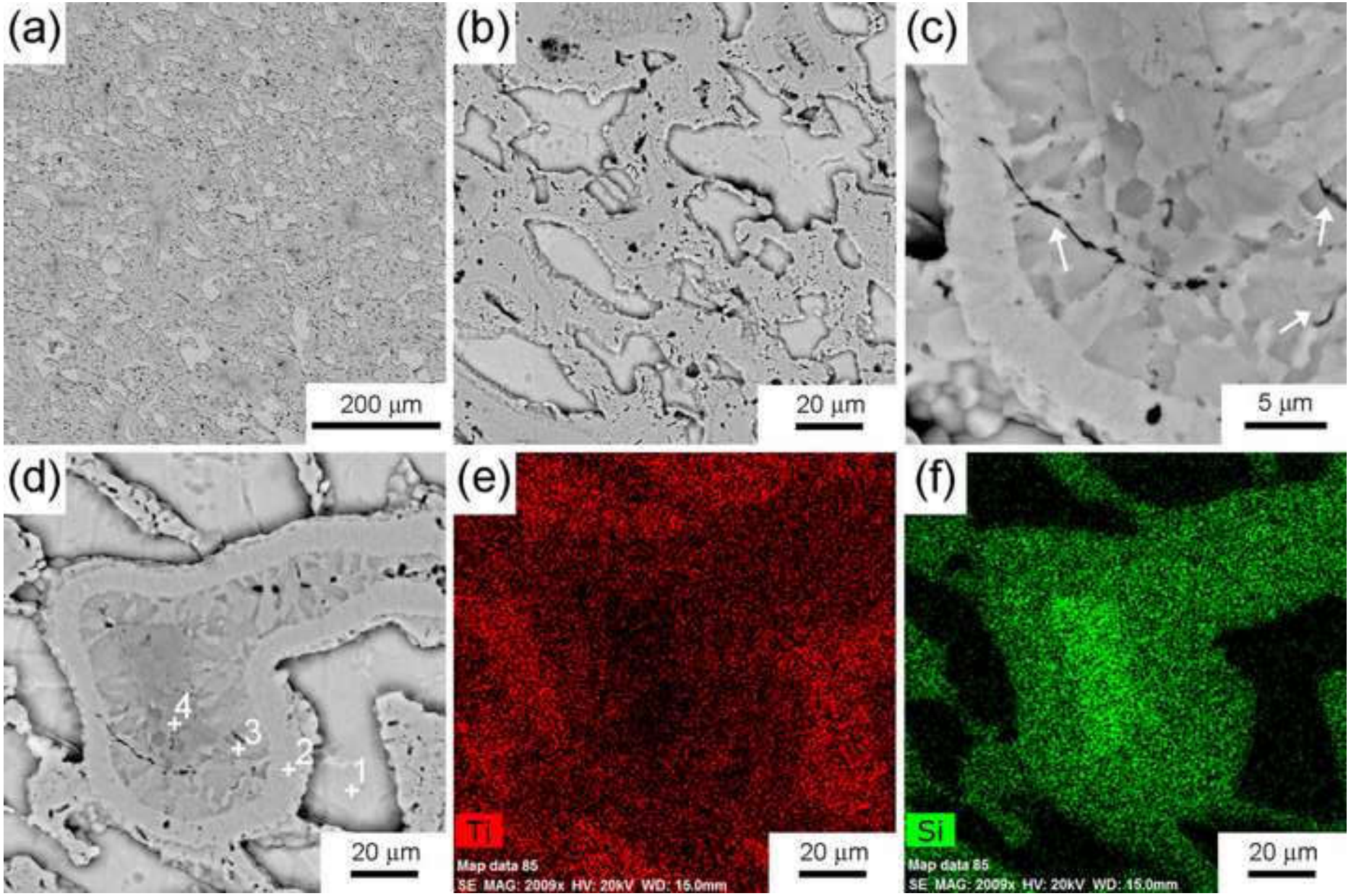

Figure 8
Click here to download high resolution image

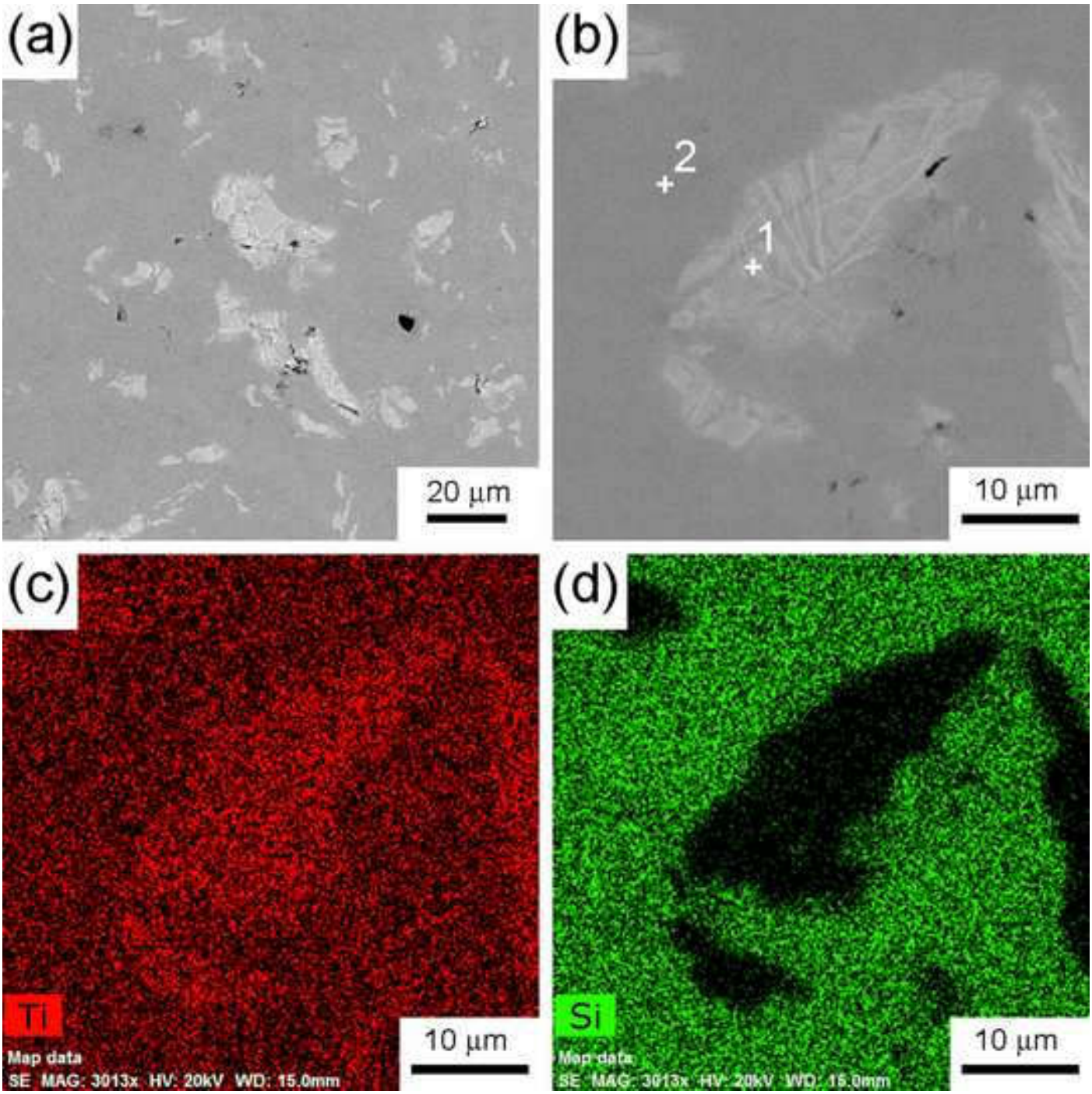

Figure 9
Click here to download high resolution image

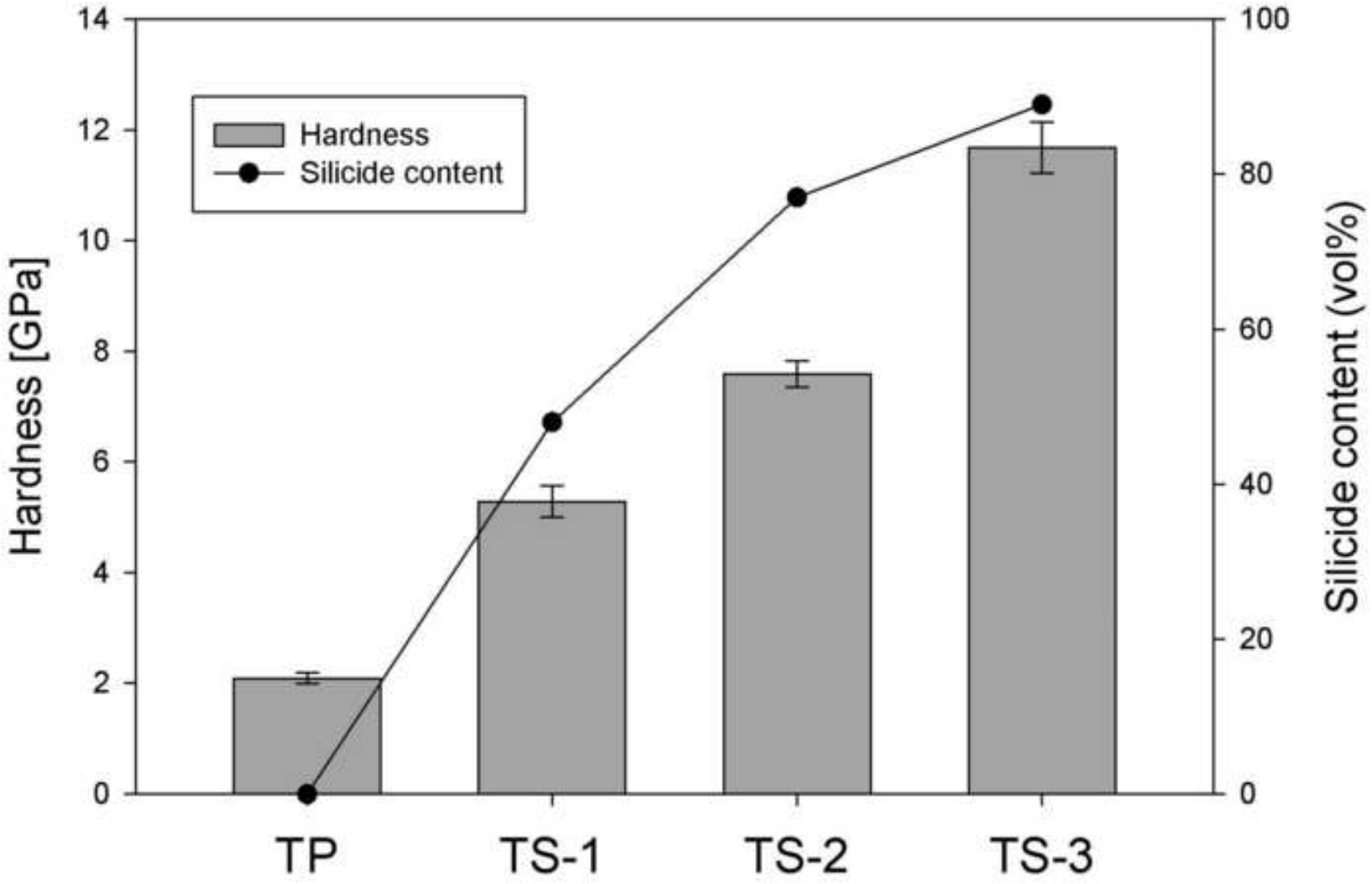

Figure 10
Click here to download high resolution image

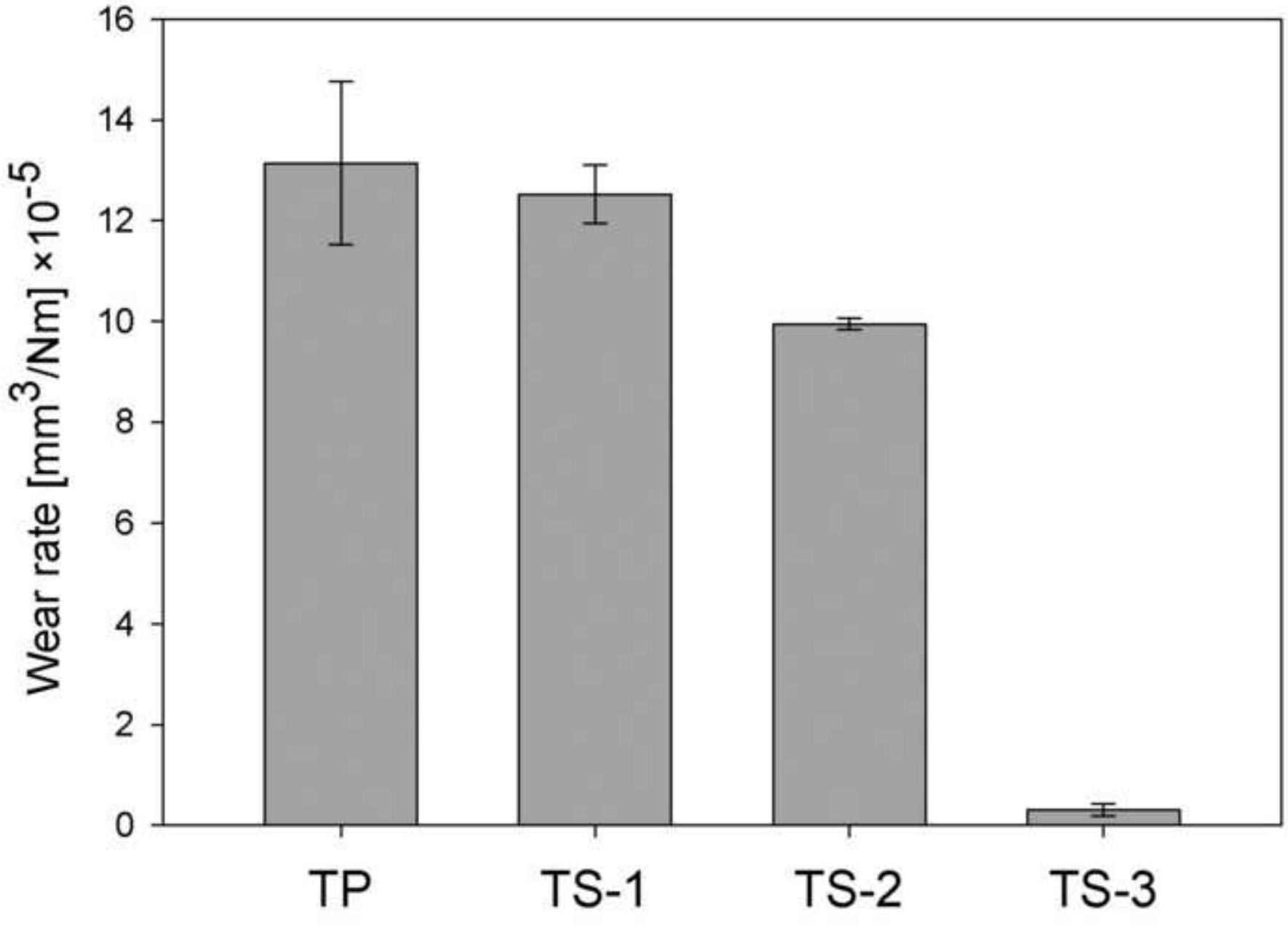

Figure 11
Click here to download high resolution image

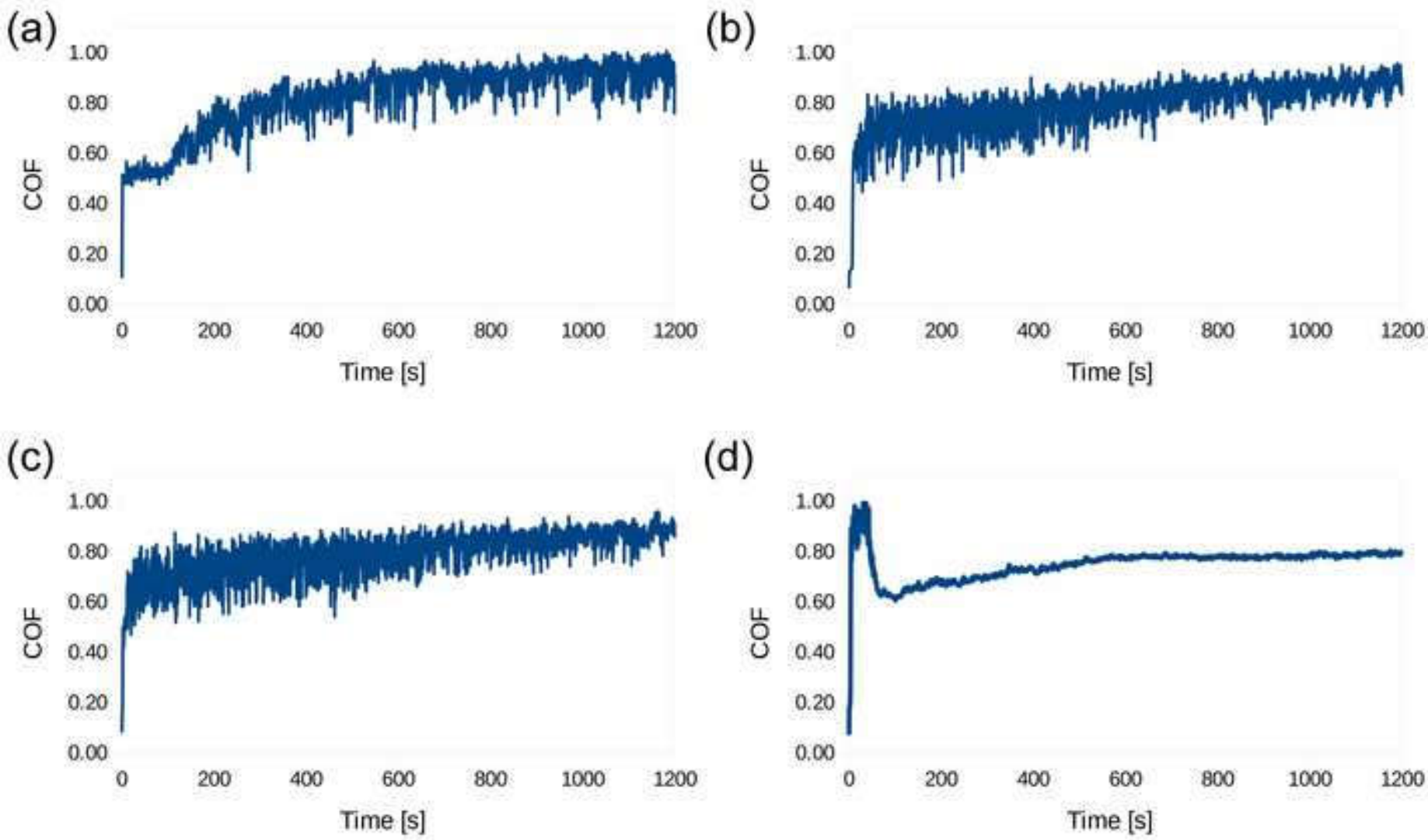

Figure 12
Click here to download high resolution image